RSC Advances

This is an *Accepted Manuscript*, which has been through the Royal Society of Chemistry peer review process and has been accepted for publication.

Accepted Manuscripts are published online shortly after acceptance, before technical editing, formatting and proof reading. Using this free service, authors can make their results available to the community, in citable form, before we publish the edited article. This *Accepted Manuscript* will be replaced by the edited, formatted and paginated article as soon as this is available.

You can find more information about *Accepted Manuscripts* in the Information for Authors.

Please note that technical editing may introduce minor changes to the text and/or graphics, which may alter content. The journal's standard Terms & Conditions and the Ethical guidelines still apply. In no event shall the Royal Society of Chemistry be held responsible for any errors or omissions in this *Accepted Manuscript* or any consequences arising from the use of any information it contains.

ROYAL SOCIETY OF CHEMISTRY

www.rsc.org/advances

Graphical Abstract

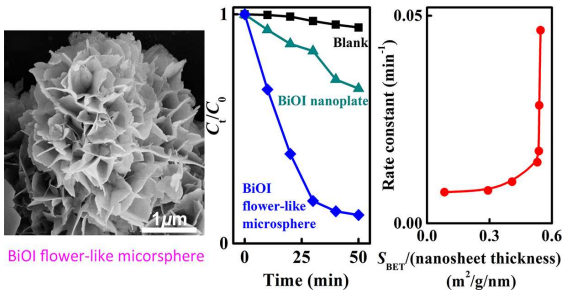

BiOI flower-like microspheres prepared using $N(Bu)_4I$ as iodine source and template exhibit high photocatalytic activity under visible light.

RSC Advances Accepted Manuscript

Synthesis, characterization, and visible-light photocatalytic activity of BiOI hierarchical flower-like microspheres

Jingyi Liu [a], Haiping Li [b], Na Du [c], Shue Song [c], Wanguo Hou [c] *

[a] *Environment Research Institute, Shandong University, Jinan 250100, P.R. China;*

[b] *National Engineering Technology Research Center for Colloidal Materials, Shandong University, Jinan 250100, P.R. China;*

[c] *Key Laboratory of Colloid and Interface Chemistry (Ministry of Education), Shandong University, Jinan 250100, P.R. China*

* To whom correspondence should be addressed

Email: wghou@sdu.edu.cn

Tel: +86-531-88365460

Fax: +86-531-88364750

RSC Advances Accepted Manuscript

Abstract

BiOI hierarchical flower-like microspheres were hydrothermally prepared, using tetrabutylammonium iodide as an iodine source and template. Many BiOI hierarchical structures have been synthesized using KI, NaI, HI or ionic liquids as the iodine source, but the use of alkyl ammonium iodide as the iodine source was not reported in the literature. The so-obtained BiOI samples were characterized by X-ray diffraction, scanning electron microscopy, transmission electron microscopy, nitrogen sorption measurements, and ultraviolet-visible diffuse reflectance spectroscopy. The effects of hydrothermal temperature and time on the BiOI crystal structure and morphology were investigated. The BiOI microspheres were composed of BiOI nanosheets. The photocatalytic performance of the BiOI samples was determined from the degradation of Rhodamine B, under visible light irradiation. BiOI microspheres prepared at 160 °C over 30 h exhibited excellent photodegradation efficiency, which was more than five and seven times higher than those of BiOI nanoplates and N-doped TiO_2, respectively. The high photocatalytic performance was attributed to the high specific surface area and low nanosheet thickness. A morphologic factor was proposed to represent the ratio of specific surface area to nanosheet thickness, and correlated to the photodegradation efficiency of the BiOI samples. The photocatalytic efficiency increased with increasing morphologic factor. The BiOI photocatalyst exhibited excellent stability and reusability, and has potential in environment remediation.

Keywords: BiOI, flower-like microsphere, photocatalysis, hierarchical structure

RSC Advances Accepted Manuscript

1. Introduction

Environmental pollution currently receives global attention [1-2], and new technologies and materials are continually being developed to assist with this problem. The photodegradation of pollutants by semiconductor photocatalysts is a promising approach, which has evoked great interest among scientists [3-6]. TiO_2 has received tremendous attention throughout the last two decades, because of its wide availability and low toxicity [7-9]. TiO_2 has a wide band gap (3.2 eV), so is responsive to ultraviolet wavelengths. It exhibits low photocatalytic activity under sunlight conditions, which limits its use [10-12]. Developing efficient visible light photocatalysts is of great importance.

BiOI has a narrow band gap (1.77–1.92 eV), and has attracted much interest as a visible light photocatalyst for pollutant degradation [13-16]. It is a ternary compound with a layered structure, characterized by $[Bi_2O_2]^{2+}$ slabs interleaved by double slabs of iodine atoms [17-19]. Several BiOI nanostructures have been reported, including nanoplates [20-22] and three-dimensional (3D) hierarchical microspheres [23-27]. Zhang et al. synthesized flower-like BiOI nanoplates via an ethylene glycol (EG)-assisted solvothermal process at 170 °C [25]. Xia et al. fabricated BiOI porous microspheres by a reactable ionic liquid (1-butyl-3-methylimidazolium iodine) assisted solvothermal method [26]. Ren et al. prepared hollow flower-like microspheres with the assistance of polyvinylpyrrolidone and citric acid through a solvothermal process at 70 °C [27]. These BiOI hierarchical structures were synthesized using KI, NaI, HI or ionic liquids as the iodine source [25-34], but the use

RSC Advances Accepted Manuscript

of alkyl ammonium iodide as the iodine source was not reported in the literature.

Herein, we report the hydrothermal synthesis of BiOI flower-like microspheres, in which tetrabutylammonium iodide (TBAI) was used as an iodine source and template. To the best of our knowledge, this is the first report of a BiOI hierarchical structure synthesized using an alkyl ammonium iodide as the iodine source. The effects of hydrothermal reaction temperature (T_H) and time (t_H) on the crystal structure, morphology, and photocatalytic performance of the BiOI samples were investigated. The BiOI flower-like microspheres exhibited higher photocatalytic activity than BiOI nanoplates and N-doped TiO_2 (N-TiO_2), and have potential in environment remediation.

2. Experimental

2.1. Materials

$Bi(NO_3)_3 \cdot 5H_2O$, KI, urea, and ethanol were of AR grade and purchased from Aladdin (P. R. China). Commercial P25 TiO_2 was purchased from Degussa (Germany). TBAI was of AR grade and purchased from Sinopharm (P. R. China). All chemicals were used as received. Ultrapure water obtained from a Hitech-Kflow water purification system (Hitech, P. R. China) was used throughout experiments.

2.2. Preparation of BiOI flower-like microspheres

0.1 g of $Bi(NO_3)_3 \cdot 5H_2O$ in 20 mL of ethanol was stirred for 15 min, and the pH of the $Bi(NO_3)_3$ precursor was 1.42. 0.076 g of TBAI in 20 mL of water was added dropwise under stirring. The color of the suspension gradually changed from yellow to red, and the pH of the system changed to 2.13. After stirring for 20 min, the

RSC Advances Accepted Manuscript

mixture was transferred to an 80-mL polytetrafluoroethylene-lined stainless steel autoclave, and heated to T_H for different t_H. The product was collected by filtration, washed thoroughly with water, and dried at 60 ºC for 12 h. The prepared products were denoted as Bi-T_H/t_H. In addition, BiOI nanoplates (denoted Bi-p) were prepared with KI as an iodine source via a similar process (S1, Supporting Information). N-TiO_2 was synthesized according to the literature [35] (S2, Supporting Information).

2.3. Characterization

Powder X-ray diffraction (XRD) patterns were recorded using a D8 Advance diffractometer (Bruker, Germany), with Cu Kα radiation (λ = 1.54184 Å). Field-emission scanning electron microscopy (SEM) images were collected using a Supra55 microscope (ZEISS, Germany). Transmission electron microscopy (TEM) and high-resolution TEM (HRTEM) images were collected using a Jeol JEM-2100F microscope (Japan). Specific surface areas (S_{BET}) were determined by measuring volumetric N_2 adsorption-desorption isotherms at liquid nitrogen temperature, using an ASAP 2020 HD88 instrument (Micromeritics, USA). Ultraviolet-visible diffuse reflectance spectra (DRS) were recorded on a Cary 100 spectrophotometer (Agilent, USA) with a $BaSO_4$ reference. Dynamic light scattering (DLS) analyses were carried out at 25 °C, using a Brookhaven Model (BI-200SM) instrument equipped with an Ar laser lamp (300 mW at 532 nm).

2.4. Photocatalytic activity measurements

The photocatalytic performance of the as-prepared catalysts under visible light irradiation was evaluated by degrading RhB at room temperature, using a XPA-7

RSC Advances Accepted Manuscript

photocatalytic reaction apparatus (Xujiang Electromechanical Plant, P. R. China). A 400-W metal halide lamp was used as the light source, and was equipped with an ultraviolet cutoff filter ($\lambda \geq 420$ nm) to provide visible light. The distance between the lamp and glass tubes containing dye solutions was ~10 cm. A water filter around the lamp was used to absorb infrared light. The reaction tubes around the lamp were soaked in a bath with temperature of 20 °C. In a typical process, 0.01 g of BiOI was dispersed in 50 mL of aqueous solution containing 10 mg/L of RhB. Prior to irradiation, the suspension was magnetically stirred, with a stirring rate of 1000 rpm, in dark for 30 min to achieve sorption equilibrium of RhB on the catalyst surface. Approximately four microliters aliquots of suspension were removed from the reaction tube every 10 min, and centrifuged (7100 ×g) for 5 min to remove particles. The pH values of suspensions were 7.3 ± 0.2 at the beginning and increased to 7.7 ± 0.1 after reactions. The RhB concentration was determined using a SP-1105 visible spectrophotometer (Spectrum, P. R. China), by measuring the absorbance at 554 nm. The ratio of the RhB concentration to its initial concentration (C/C_0) was obtained by calculating the ratio of the corresponding absorbances.

3. Results and Discussion

3.1. XRD analysis

Figure 1 shows XRD patterns of the BiOI samples prepared at different T_H and t_H. Retaining T_H at 160 °C while varying t_H from 6 to 48 h, resulted in all samples exhibiting the characteristic peaks of highly crystalline BiOI (Fig. 1a). Peaks at 19.3, 29.6, 31.7, 37.1, 39.3, 45.5, 51.4, 55.2, 60.2, and 66.3° corresponded to the (002),

RSC Advances Accepted Manuscript

(012), (110), (013), (004), (014), (114), (212), (115), and (220) planes, respectively, and were indexed to the tetragonal phase of BiOI (JCPDS Card no. 10-0445). No peaks of impurities were observed. Among these BiOI samples, Bi-160/30 exhibited the highest intensity XRD peaks, suggesting it possessed the highest crystallinity. Bi-p exhibited a similar XRD pattern (Fig. S1, Supporting Information). The effect of T_H was investigated at a constant t_H of 30 h (Fig. 1b). Decreasing T_H to 120 °C or increasing to 180 °C (from the initial T_H of 160 °C) resulted in decreased crystallinity, as indicated by decreased XRD peak intensities. Thus, the optimal T_H and t_H for preparing highly crystalline BiOI were 160 °C and 30 h, respectively.

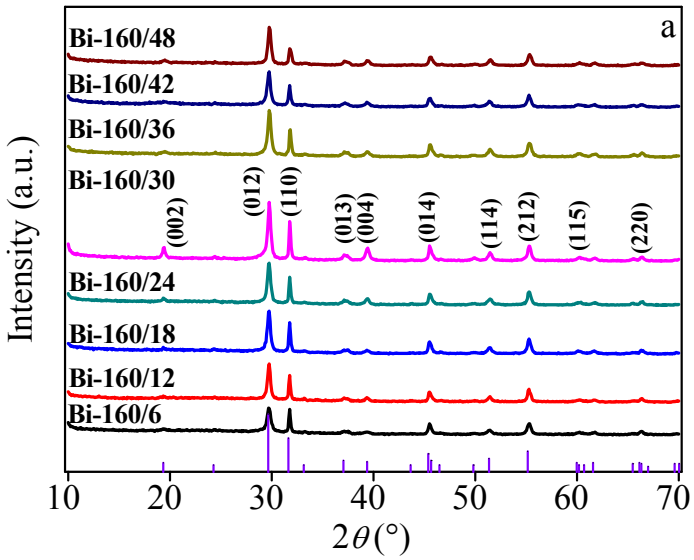

RSC Advances Accepted Manuscript

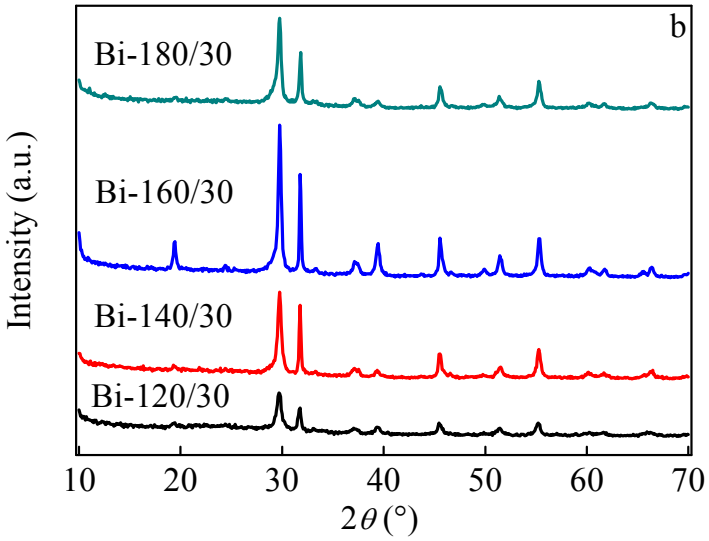

Fig. 1 XRD patterns of BiOI samples prepared at (a) 160 °C for t_H and (b) different T_H for 30 h.

In addition, the average crystallite sizes of the BiOI samples were calculated from the (012) peaks of the XRD patterns using the Scherrer formula, and were in the range of 17.9–29.5 nm (Fig. S2, Supporting Information). No obvious trend in average crystallite sizes was observed with either T_H or t_H.

3.2. SEM and TEM analyses

Figure 2 shows SEM and TEM images of the BiOI samples. Non-uniform nanoplates were observed for Bi-p (Fig. 2a and c), which had an average size and thickness of about 1–2 μm and 65.7 nm, respectively. Bi-160/30 exhibited a morphology consisting of three-dimensional, hierarchical, flower-like microspheres, with diameters of ~2 μm (Fig. 2b and d). These flower-like BiOI microspheres were constructed from nanosheets of average thickness ~26.4 nm (Fig. 2b). Insets in Fig. 2c and d showed HRTEM images of Bi-p and Bi-160/30, respectively. The observed lattice fringe spacing of 0.282 nm was corresponded to (110) facets.

RSC Advances Accepted Manuscript

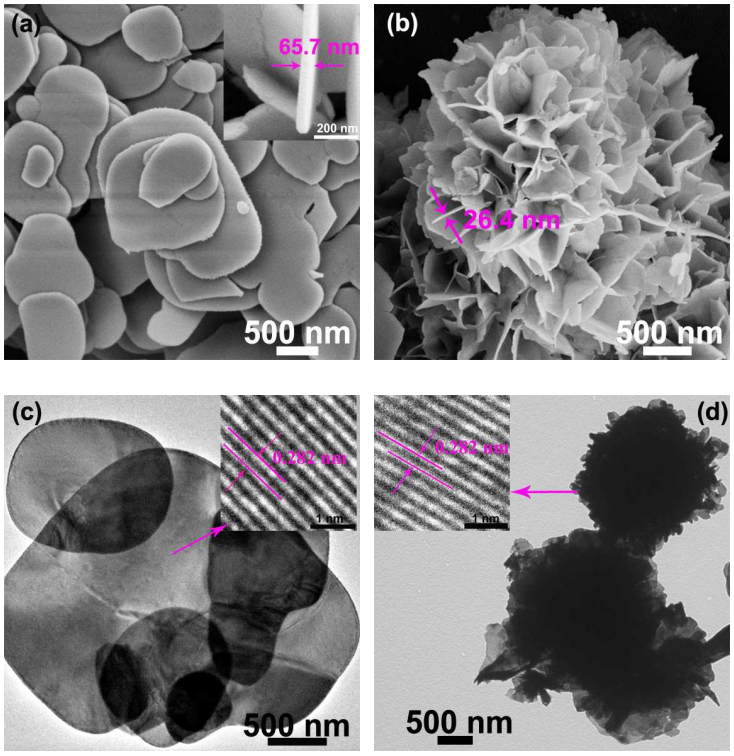

Fig. 2 (a, b) SEM and (c, d) TEM images of (a, c) Bi-p and (b, d) Bi-160/30. Insets show HRTEM images.

To investigate intermediates and the formation mechanism of the flower-like microspheres, a time-evolution experiment was conducted at T_H of 160 °C, to track the morphologic change of BiOI crystals. The reagents and precursors were first characterized, so that the change in morphology of the products could be better understood. The average hydrodynamic diameter of TBAI micelles (or aggregates) in solution was ~102 nm, as measured by DLS (Fig. S3, Supporting Information). $Bi(NO_3)_3$ in ethanol exhibited irregular flake particles (Fig. 3a). Mixing $Bi(NO_3)_3$ with H_2O resulted in a rapid reaction producing $BiONO_3$ [36]. $BiONO_3$ was prepared by mixing the ethanol dispersion of $Bi(NO_3)_3$ and water, and exhibited disc-shaped particles of size ~1.5 μm, which appeared to consist of flakes (Fig. 3b). Both the

RSC Advances Accepted Manuscript

ethanol dispersion of $Bi(NO_3)_3$ and the TBAI micelle solution were colorless. Mixing these two systems immediately produced a brown dispersion. The SEM image of the resulting BiOI (Bi-25/0) showed nanosheets of thickness ~73.9 nm (Fig. 3c). This was significantly different from the morphologies of $BiONO_3$ and $Bi(NO_3)_3$ in ethanol (Fig. 3a and b). This suggested that the formation of BiOI was very quick, which was supported by XRD measurements (Fig. S4, Supporting Information). No characteristic reflections of $BiONO_3$ were observed in the XRD patterns of any BiOI sample.

After hydrothermal treatment at 160 °C for 1 h, only irregular BiOI nanosheets were observed (Fig. 3d). This suggested that no obvious change in BiOI morphology occurred. When the t_H was increased to 6 h, rudiments of the flower-like microspheres were formed by the nanosheets (Fig. 3e). These flower-like rudiments gradually grew with increasing t_H (Fig. 3f). When t_H was >18 h, integral flower-like microspheres were formed (Figs. 2b, 3g, 3h, and 3i). Increasing t_H to above 36 h caused some degree of destruction to the microsphere structure (Fig. 3j and k), which resulted in loose aggregates. The influence of T_H on the morphology of BiOI was also investigated at t_H of 30 h. No integral flower-like microspheres were obtained at T_H of 120, 140, and 180 °C, as shown in Figs. 3l, m, and n, respectively. This suggested that a T_H of 160 °C was suitable for forming the flower-like microspheres.

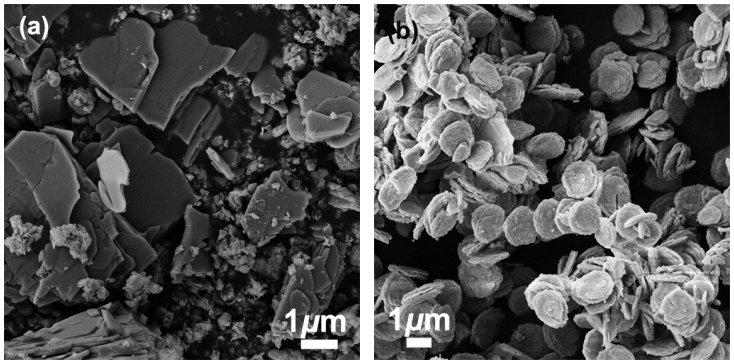

RSC Advances Accepted Manuscript

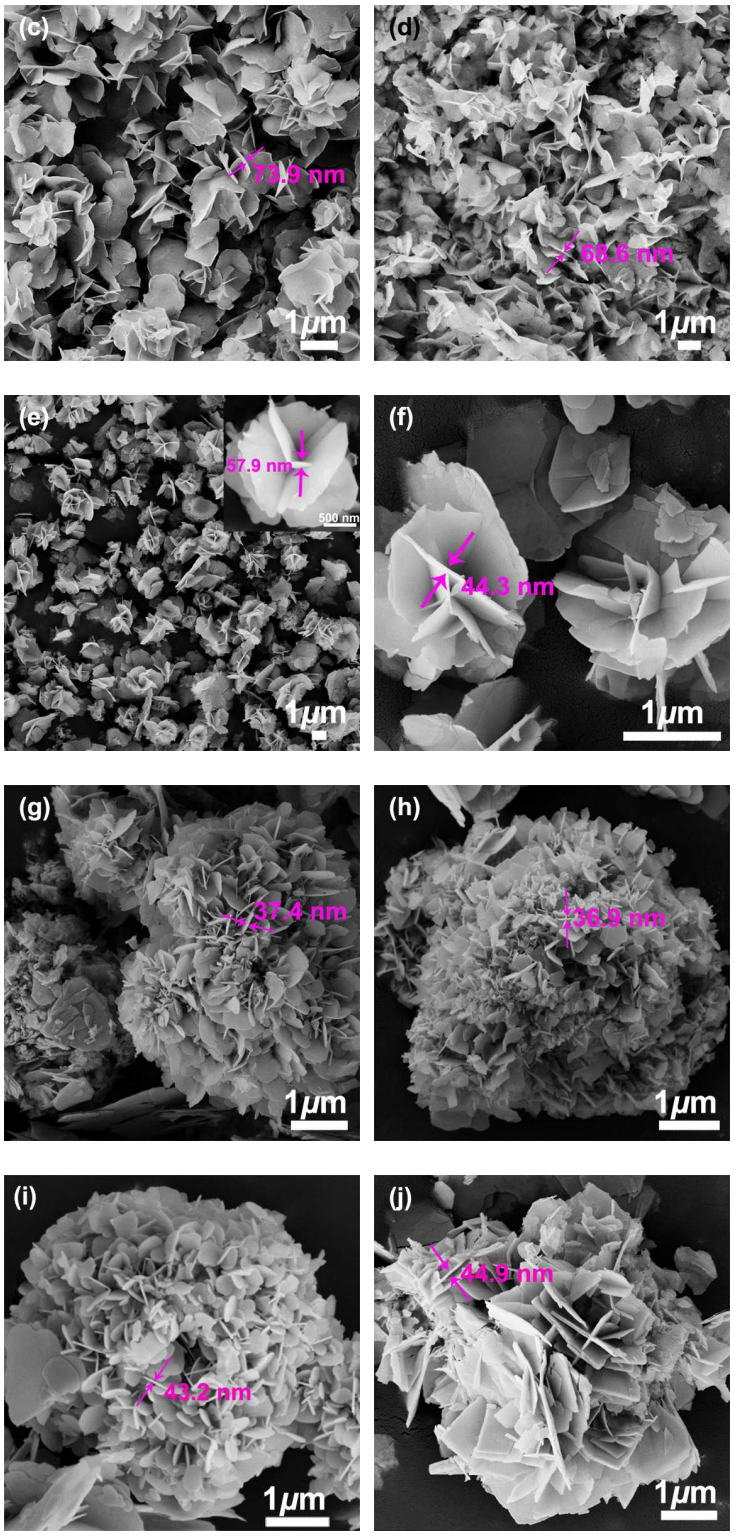

RSC Advances Accepted Manuscript

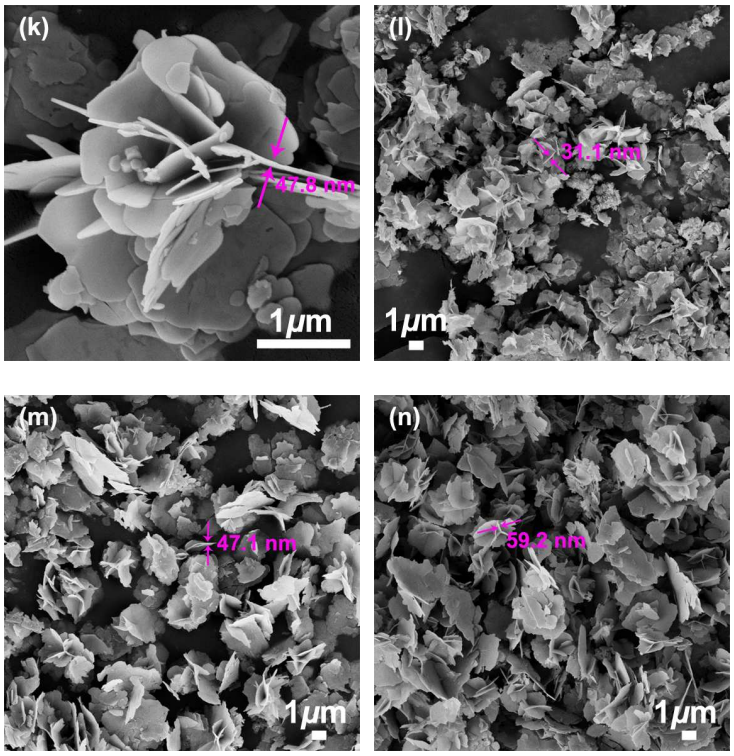

Fig. 3 SEM images of (a) $Bi(NO_3)_3$, (b) $BiONO_3$, (c) Bi-25/0, (d) Bi-160/1, (e) Bi-160/6, (f) Bi-160/12, (g) Bi-160/18, (h) Bi-160/24, (i) Bi-160/36, (j) Bi-160/42, (k) Bi-160/48, (l) Bi-120/30, (m) Bi-140/30, and (n) Bi-180/30.

Based on the above discussion, a possible formation mechanism of the flower-like microspheres is proposed, as illustrated in Scheme 1. Mixing the ethanol dispersion of $Bi(NO_3)_3$ and TBAI micelle solution caused the TBAI micelles to act as reaction centers. The reaction between I^- and $Bi_2O_2^{2+}$ formed BiOI nuclei at the micelle surface. These nuclei gradually grew into nanosheets embedded in the micelles, to form aggregates. Dissolution-recrystallization occurred during hydrothermal treatment, causing the nanosheets to gradually bond, forming flower-like rudiments and then compact microspheres. The flower-like BiOI microspheres were retained after washing out the TBAI cations. In this process, TBAI

RSC Advances Accepted Manuscript

functioned as an iodine source and template. Excess t_H resulted in Ostwald ripening, where larger sheets continued to grow and smaller ones disappeared. This may have been responsible for the partial destruction of the microsphere structure.

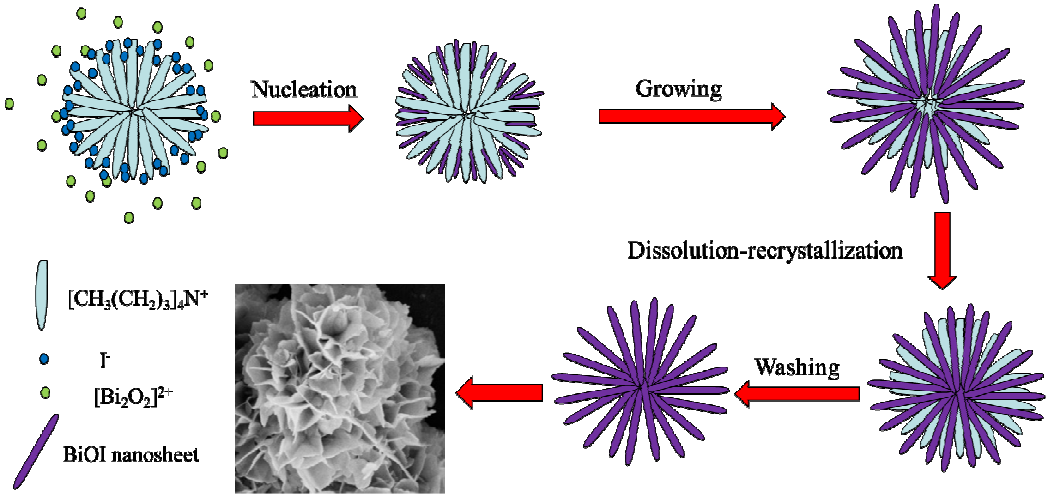

Scheme 1 Proposed formation mechanism of the BiOI flower-like microspheres.

All BiOI samples obtained at different T_H and t_H exhibited hierarchical structures constructed from many nanosheets (Figs. 2 and 3). The average thicknesses of a nanosheet in each BiOI sample (H_{ns}) was measured from >50 nanosheets for each sample, and the results are shown in Fig. 4. Increasing t_H at a constant T_H of 160 °C resulted in the H_{ns} of the Bi-160/t_H samples to gradually decrease and then increase. Bi-160/30 exhibited the lowest H_{ns}. Samples prepared at higher and lower T_H exhibited increased H_{ns}. The reason for the change in H_{ns} with T_H and t_H has not yet been resolved.

RSC Advances Accepted Manuscript

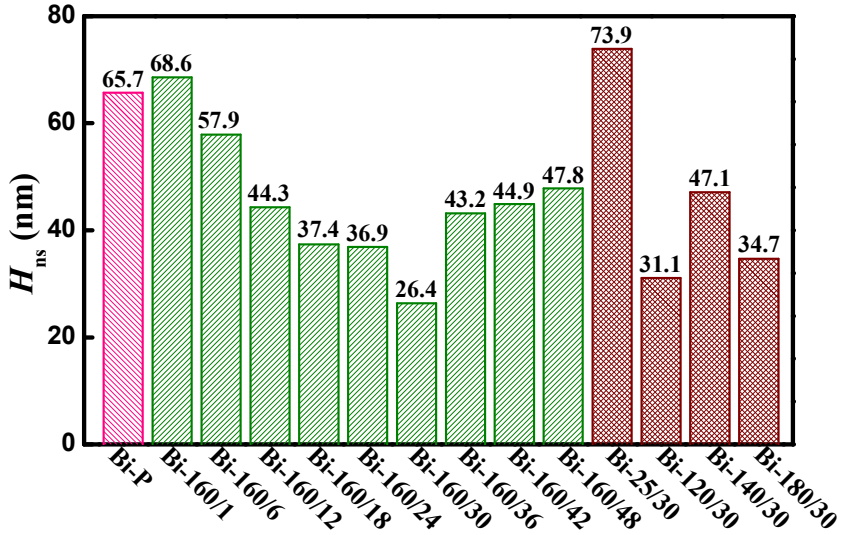

Fig. 4 Average nanosheet thicknesses of BiOI samples.

3.3. N_2 sorption isotherms

N_2 adsorption-desorption isotherms were measured to determine the S_{BET} of the BiOI-T_H/t_H and Bi-p samples, and the results are shown in Fig. 5. All isotherms were of type IV with H3 hysteresis loops [37-38], which were characteristic of mesoporous materials. S_{BET} (m^2/g) values were analyzed by the Brunauer-Emmett-Teller (BET) method, from the adsorption branch of the isotherms, and the results are also shown in Fig. 5. No obvious trend in S_{BET} was observed with increasing T_H at constant t_H of 30 h, or with increasing t_H at constant T_H of 160 °C. The S_{BET} of Bi-160/30 was 14.4 m^2/g, which was twice more than that of Bi-p (5.5 m^2/g).

RSC Advances Accepted Manuscript

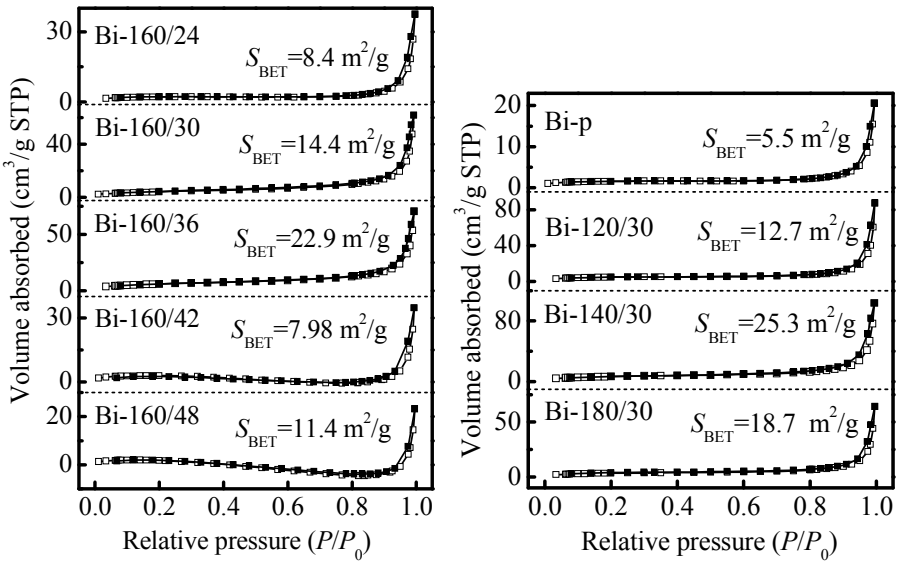

Fig. 5 N_2 adsorption-desorption isotherms and S_{BET} values of BiOI samples.

3.4. Optical absorption properties

The optical properties of the BiOI samples were investigated by ultraviolet-visible DRS, and are shown in Fig. 6. Bi-p and Bi-160/30 exhibited absorption edges up to ~650 nm, which indicated a small band gap. An absorption peak at ~450 nm was also exhibited by both samples. The band gaps of crystalline semiconductors can be calculated from their absorption spectra according to:

$$\alpha h\nu = K (h\nu - E_g)^{n/2}, \quad (1)$$

where K, α, ν, and E_g are the proportionality constant, absorption coefficient, light frequency, and band gap, respectively. n depends on the transition characteristics of the semiconductor, and values of 1 and 4 correspond to direct and indirect band-gap semiconductors, respectively. BiOI has been shown to have an n value of 4 [39]. Thus, the band gaps of Bi-p and Bi-160/30 were determined to be about 1.81 eV (Fig. 6, inset), which are similar to reported values [13].

RSC Advances Accepted Manuscript

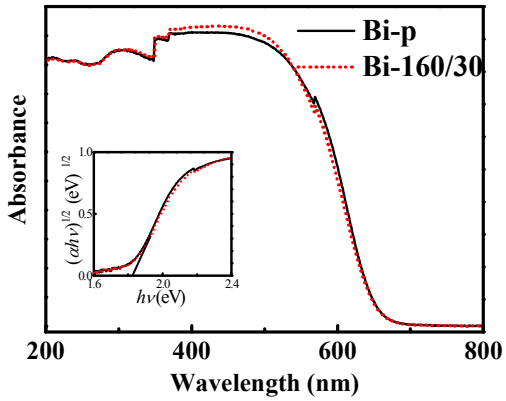

Fig. 6 Ultraviolet-visible diffuse reflectance spectra of BiOI samples. Insert shows $(\alpha h\nu)^{1/2}$ versus $h\nu$ curves.

3.5. Photocatalytic activity

The photocatalytic performance of the BiOI samples was evaluated by degrading RhB under visible light irradiation, and was compared with that of N-TiO_2 and P25 TiO_2. The results are shown in Fig. 7(a) and (b). No obvious degradation of RhB was observed in the absence of a photocatalyst. Bi-160/30 exhibited the highest photocatalytic efficiency among the tested catalysts. Approximately 88% of RhB was degraded by Bi-160/30 after 50 min.

The pseudo-first-order kinetics model was used to fit the photodegradation data, the equation for which is:

$$-\ln(C_t/C_0) = kt, \quad (2)$$

where k and t are the apparent first-order rate constant and irradiation time, respectively. The model fitting plots and corresponding k values are shown in Fig. 7(c) and (d), respectively. Bi-160/30 exhibited the highest k, which was 5, 7, and 20 times higher than those of Bi-p, N-TiO_2 and P25 TiO_2, respectively.

RSC Advances Accepted Manuscript

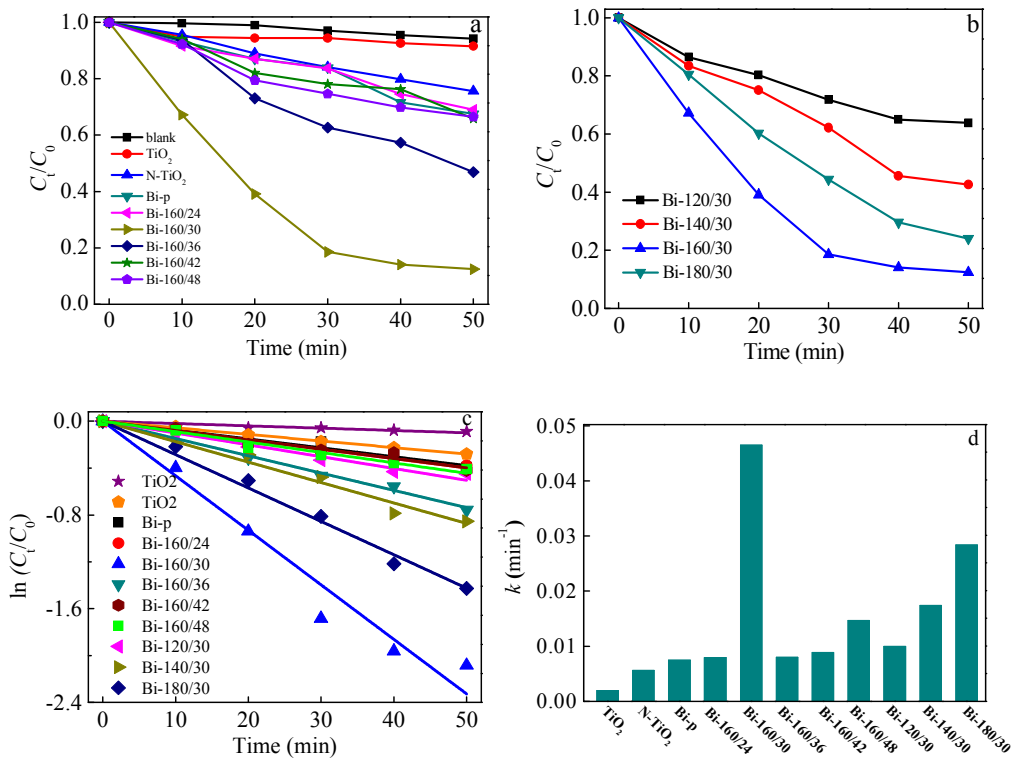

Fig. 7 (a, b) Photocatalytic degradation of RhB, (c) pseudo first-order kinetics fitting plots and (d) apparent first-order rate constants for various photocatalysts.

The effect of pH on the photodegradation activity of Bi-160/30 was studied (Fig. S5, Supporting Information). The degradation rate almost kept constant at pH 3–7.5, but dramatically decreased at pH > 8. The isoelectric point of the BiOI sample is pH 7.72. The decrease of degradation rate at pH > 8 was probably ascribed to the decreased RhB adsorption on the surface of Bi-160/30 owing to the high electrostatic repulsion between RhB and Bi-160/30.

Stability and reusability are important considerations for the use of photocatalysts in practical application. Fig. 8 shows cycling experiments for RhB

RSC Advances Accepted Manuscript

degradation by Bi-160/30. After three consecutive runs, the photocatalytic efficiency of Bi-160/30 declined by < 6%. The XRD patterns and SEM images showed that the structure and morphology of Bi-160/30 remained largely constant throughout the three cycles (Fig. 9). Thus, Bi-160/30 exhibited high stability and reusability during the photocatalytic reactions.

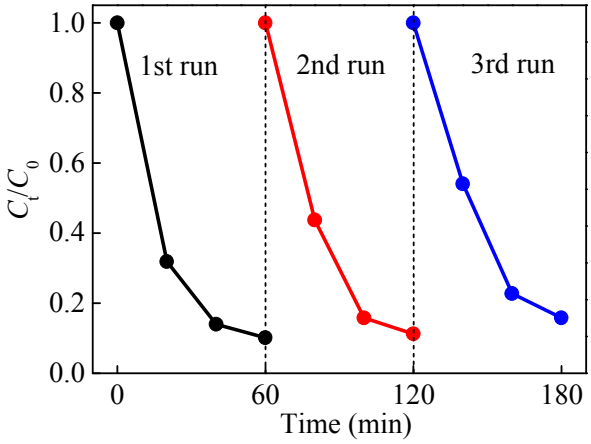

Fig. 8 Three consecutive RhB degradation cycles by Bi-160/30.

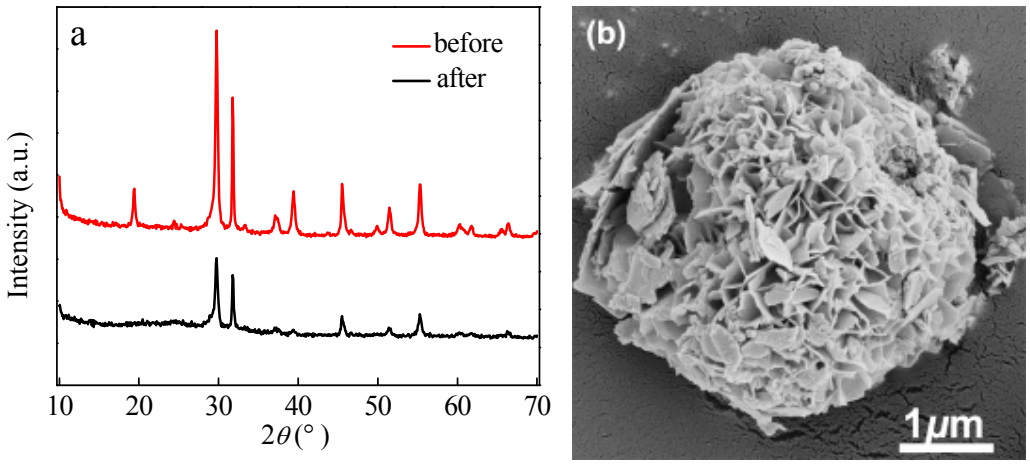

Fig. 9 (a) XRD patterns and (b) SEM image of Bi-160/30 after three consecutive

RSC Advances Accepted Manuscript

298 photocatalytic degradations of RhB.

299

300 Understanding the effect of a photocatalysts morphology on its photocatalytic
301 performance is of theoretical and practical importance. Large specific surface areas
302 and low lamella thicknesses for flaky photocatalysts generally enhance photocatalytic
303 performance [40-41]. Large specific surface areas favor the adsorption of more
304 organic pollutants, and provide more reactive sites on the photocatalyst surface [42].
305 Low lamella thicknesses can allow photogenerated electrons and holes to transfer to
306 the particle surface in a shorter distance, and thus decrease the recombination of
307 electrons and holes [43-44]. The amount of adsorbed RhB on the BiOI samples
308 increased with increasing S_{BET} (Fig. S6, Supporting Information). However, no
309 obvious trend in k was observed with either S_{BET} or H_{ns} (Fig. S7, Supporting
310 Information). This was because S_{BET} and H_{ns} were not constant for the BiOI samples.
311 k was found to correlate well with S_{BET}/H_{ns}, as shown in Fig. 10. With increasing
312 S_{BET}/H_{ns}, k gradually increased, and then dramatically increased at S_{BET}/H_{ns} > ~0.53
313 $m^2/(g \cdot nm)$. S_{BET}/H_{ns} represented the ratio of specific surface area to lamella thickness,
314 and was referred to as the morphologic factor (F_m). F_m reflected the effects of S_{BET}
315 and H_{ns} on the photocatalytic performance of the photocatalysts.

RSC Advances Accepted Manuscript

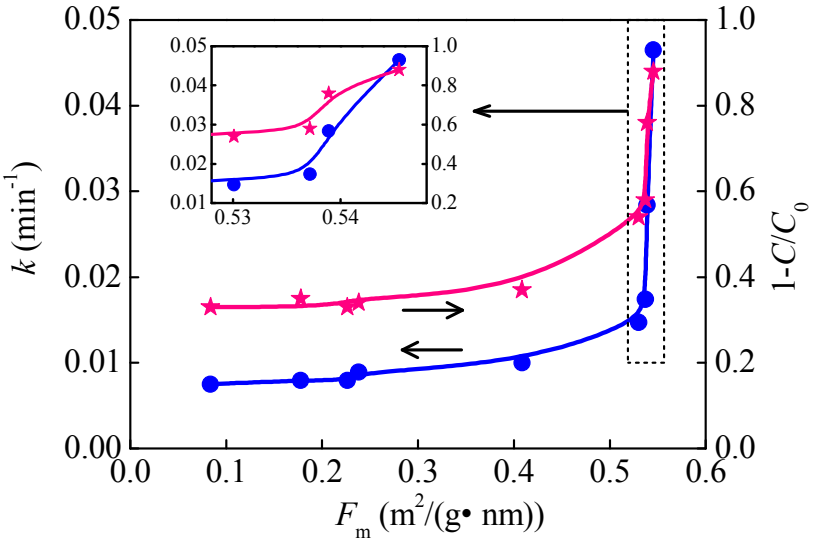

316

317 **Fig. 10** Dependence of rate constant and degraded RhB percentage on F_m.

318

319 The photodegradation of organic pollutants may involve one or more of the
320 active species •OH, h^+, $•O_2^-$ and e^- [45]. To investigate the contributions of these
321 active species, different scavengers were added to the photocatalytic degradation
322 reaction, with Bi-160/30 used as the model photocatalyst. Tert-butyl alcohol (*t*-BuOH)
323 was used as the scavenger for •OH [46], sodium oxalate for h^+ [47], benzoquinone
324 (BQ) for $•O_2^-$ [46], and potassium dichromate for e^- [48]. Fig. 11 shows the effects of
325 the scavengers on the photocatalytic efficiency. In the presence of *t*-BuOH or $K_2Cr_2O_7$,
326 the photocatalytic efficiency of Bi-160/30 was slightly reduced, indicating that •OH
327 and e^- were not significant in the photodegradation process. When BQ or sodium
328 oxalate was added to the dispersion, the photocatalytic activity of Bi-160/30
329 decreased significantly, indicating that $•O_2^-$ and h^+ played important roles. Therefore,
330 $•O_2^-$ and h^+ were the main active species for RhB degradation by BiOI, in agreement

RSC Advances Accepted Manuscript

331 with previous reports [49].

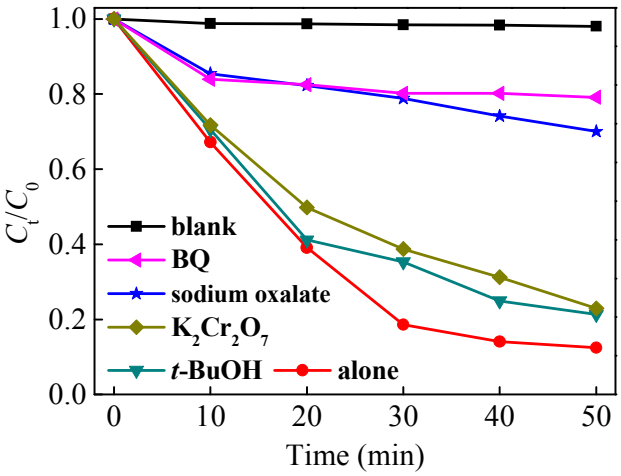

332

333

334 **Fig. 11** Photodegradation efficiency of RhB over Bi-160/30, in the
335 presence of different scavengers: 20 mM *t*-BuOH, 0.2 mM
336 sodium oxalate, 10 mM $K_2Cr_2O_7$, and 0.1 mM BQ.

337 ## 4. Conclusions

338 Three-dimensional, hierarchical, flower-like BiOI microspheres were
339 hydrothermally prepared, using TBAI as an iodine source and template for the first
340 time. The BiOI microspheres had an average diameter of ~2 μm, and consisted of
341 BiOI nanosheets. The photocatalytic performance of the BiOI samples was influenced
342 by their specific surface area and nanosheet thickness. F_m was used to describe the
343 photodegradation performance of the BOI samples, with photocatalytic efficiency
344 increasing with increasing F_m. Bi-160/30 exhibited the highest photodegradation
345 efficiency for RhB under visible light irradiation, which was five and seven times
346 more than those of Bi-p and N-TiO_2, respectively. Bi-160/30 exhibited good stability
347 and reusability.

RSC Advances Accepted Manuscript

Acknowledgements

The present work is supported financially by the National Natural Science Foundation of China (No. 21173135) and the Specialized Research Fund for the Doctoral Program of Higher Education of China (No. 20110131130008).

RSC Advances Accepted Manuscript

References

[1] K. Maeda, T. Takata, M. Hara, N. Saito, Y. Inoue, H. Kobayashi and K. Domen, *J. Am. Chem. Soc.*, 2005, **127**, 8286-8287.

[2] A. Hameed, T. Montini, V. Gombac, and P. Fornasiero, *J. Am. Chem. Soc.*, 2008, **130**, 9658-9659.

[3] H. Yamashita, M. Harada, J. Misaka, M. Takeuchi, K. Ikeue and M. Anpo, *J. Photochem. Photobiol. A*, 2002, **148**, 257-261.

[4] E. Bae and W. Choi, *Environ. Sci. Technol.*, 2003, **37**, 147-152.

[5] H. M. Jia, W. J. Xiao, L. Z. Zhang, Z. Zheng, H. L. Zhang and F. Deng, *J. Phys. Chem. C*, 2008, **112**, 11379-11384.

[6] K. Vinodgopal and P. V. Kamat, *Environ. Sci. Technol.*, 1995, **29**, 841-845.

[7] T. Oncescu, M. I. Stefan and P. Oancea, *Environ. Sci. Pol. Res*, 2010, **17**, 1158-1166.

[8] M. Kong, Y. Li, X. Chen, T. Tian, P. Fang, F. Zheng and X. Zhao, *J. Am. Chem. Soc.*, 2011, **133**, 16414-16417.

[9] S. G. Kumar, L. G. Devi, *J. Phys. Chem. A*, 2011, **115**, 13211-13241.

[10] Y. N. Wang, K. J. Deng and L. J. Deng, *J. Phys. Chem. C*, 2011, **115**, 14300-14308.

[11] R. Hao, X. Xiao, X. Zuo, J. Nan and W. Zhang, *J. Hazard. Mater.*, 2012, **209**, 137-145.

[12] Y. Lei, G. Wang, S. Song, W. Fan and H. Zhang, *CrystEngComm*, 2009, **11**, 1857-1862.

RSC Advances Accepted Manuscript

[13] S. X. Ge, and L. Z. Zhang, *J. Nano. Res.*, 2012, **14**, 1-11.

[14] Y. Y. Li, J. S. Wang, H. C. Yao, L. Y. Dang and Z. J. Li, *J. Mol. Catal. A: Chem*, 2011, **334**, 116-122.

[15] T. B. Li, G. Chen, C. Zhou, Z. Y. Shen, R. C. Jin and J. X. Sun, *Dalton. Trans.*, 2011, **40**, 6751-6758.

[16] L. Q. Ye, Y. R. Su, X. L. Jin , H. Q. Xie and C. Zhang, *Environ. Sci.: Nano*, 2014, **1**, 90-112.

[17] L. Q. Ye, L. H. Tian, T. Y. Peng and L. Zan, *J. Mater. Chem.*, 2011, **21**, 12479-12484.

[18] L. Ye, J. Chen, L. Tian, J. Liu, T. Peng, K. Deng and L. Zan, *Appl. Catal. B: Environ.*, 2013, **130**, 1-7.

[19] W. L. Huang and Q. Zhu, *J. Comput. Chem.*, 2009, **30**, 183-190.

[20] J. Hu, S. Weng, Z. Zheng, Z. Pei, M. Huang and P. Liu, *J. Hazard. Mater.*, 2014, **264**, 293-302.

[21] X. Chang, J. Huang, Q. Tan, M. Wang, G. Ji, S. Deng and G. Yu, *Catal. Commun.*, 2009, **10**, 1957-1961.

[22] J. Jiang, X. Zhang, P. Sun and L. Zhang, *J. Phys. Chem. C*, 2011, **115**, 20555-20564.

[23] X. Zhang, Z. Ai, F. Jia and L. Zhang, *J. Phys. Chem. C*, 2008, **112**, 747-753.

[24] X. Xiao and, W. D. Zhang, *J. Mater. Chem.*, 2010, **20**, 5866-5870.

[25] B. Zhang, G. B. Ji, M. A. Gondal, Y. S. Liu, X. M. Zhang, X. F. Chang and N. W. Li, *J. Nano. Res.*, 2013, **15**, 1-9.

RSC Advances Accepted Manuscript

399 [26] J. Xia, S. Yin, H. M. Li, H. Xu, L. Xu, Q. Zhang, *Colloids Surf. A: Physicochem.*
400 *Eng. Aspects*, 2011, **387**, 23-28.
401 [27] K. Ren, K. Zhang, J. Liu, H. Luo, Y. Huang and X. Yu, *CrystEngComm*, 2012, **14**,
402 4384-4390.
403 [28] S. X. Wu, J. Z. Fang, X. T. Hong, K. S. Hui and Y. F Chen, *Dalton Trans.*, 2014,
404 **43**, 2611-2619.
405 [29] J. Di, J. X. Xia, S. Yin, H. Xu, L. Xu, Y. G. Xu and H. M. Li, *J. Mater. Chem. A*,
406 2014, **2**, 5340-5351.
407 [30] N Huang, A Hu, and M Li, *Mater. Lett.* 2013, **109**, 247-252.
408 [31] Z. K. Cui, M. M. Si, Z. Zheng, L. W. Mi, W. J. Fa and H. M. Jia, *Catal. Commun.*
409 2013, **42**, 121-124.
410 [32] D. K. Ma, S. M. Zhou, X. Hu, Q. R. Jiang and S. M. Huang, *Mater. Chem. Phys.*
411 2013, **140**, 11-15.
412 [33] J Cao, X Li, H. L. Lin, S. F. Chen and X Fu, *J. Hazard. Mater.* 2012, **239**,
413 316-324.
414 [34] J Cao, B. Y. Xu, B. D. Luo, H. L. Lin and S. F. Chen, *Catal. Commun.* 2011, **12**,
415 660-664.
416 [35] D. Mitoraj and H. Kisch, *Angew. Chem. Int. Ed.*, 2008, **47**, 9975-9978.
417 [36] P. V. Ioannou, *Main Group Chem.*, 2011, **10**, 255-264.
418 [37] A. Kay and I. Cesar, *J. Am. Chem. Soc.*, 2006, **128**, 15714-15721.
419 [38] Y. Li, J. Liu, X. Huang and G. Li, *Cryst. Growth Des.*, 2007, **7**, 1350-1355.
420 [39] H. F. Cheng, B. B. Huang, Y. Dai, X. Y. Qin and X. Y. Zhang, *Langmuir*, 2010,

RSC Advances Accepted Manuscript

26, 6618-6624.

[40] H. F. Cheng, B. B. Huang, Y. Dai, *Nanoscale*, 2014, **6**, 2009-2026.

[41] S. X. Yang, Q. Yue, Z. H. Chen, J. H. Yang , J. B. Li, *J. Alloys Compd.*, 2014, **597**, 91-94.

[42] J. Xia, S. Yin, H. Li, H. Xu, Y. Yan and Q. Zhang, *Langmuir*, 2010, **27**, 1200-1206.

[43] Z. Zhang, C. C. Wang, R. Zakaria and J. Y. Ying, *J. Phys. Chem. B*, 1998, **102**, 10871-10878.

[44] N. J. Huo, Q. Yue, S. X. Yang, J. B.Li, *ChemPhysChem.*, 2013, **14**, 4069-4073.

[45] J. Ryu and W. Choi, *Environ. Sci. Technol.*, 2004, **38**, 2928-2933.

[46] L. Mohapatra, K. Parida and M. Satpathy, *J. Phys. Chem. C*, 2012, **116**, 13063-13070.

[47] X. Xiao, R. Hu, C. Liu, C. Xing, C. Qian, X. Zuo and L. Wang, *Appl. Catal. B: Environ.*, 2013, **140**, 433-443.

[48] S. Ge and L. Zhang, *Environ. Sci. Technol.*, 2011, **45**, 3027-3033.

[49] H. Lee and W. Choi, *Environ. Sci. Technol.*, 2002, **36**, 3872-3878.

RSC Advances Accepted Manuscript